# Size-dependent Molecular Characteristics and Possible Sources of Organic Aerosols at a Coastal New Particle Formation Hotspot of East China

**Huan Yu[1], Yibei Wan[1], Xiangpeng Huang[2], Xinlei Ge[2], Bin Jiang[3], Yuhong Liao[3], Qian Yan[4], Qin Shuai[4], Hang Xiao[5]**

[1] School of Environmental Studies, China University of Geosciences, Wuhan, 430074, China

[2] School of Environmental Science and Engineering, Nanjing University of Information Science and Technology, Nanjing, 210044, China

[3] Guangzhou Institute of Geochemistry, Chinese Academy of Sciences, Guangzhou 510640, China

[4] School of Material Science and Chemistry, China University of Geosciences, Wuhan, 430074, China

[5] Ningbo Urban Environment Observation and Research Station, Institute of Urban Environment, Chinese Academy of Sciences, Xiamen 361021, China

Corresponding author: H. Yu (yuhuan@cug.edu.cn)

**Key Points:**

- Size-dependent organic molecular characteristics was revealed by FT-ICR-MS measurement at a coastal new particle formation hotspot.
- SPME-GC-MS analysis linked coastal ultrafine organic aerosols with VOC emission from local intertidal macroalge.
- We conducted a systematical comparison of $PM_{2.5}$ chemical composition between the coastal NPF hotspot and a typical inland urban site.

## Abstract

We investigated size-dependent molecular characteristics of coastal organic aerosols from < 0.032 μm to 3.2 μm at a new particle formation (NPF) hotspot of east China by using Fourier transform-ion cyclotron resonance mass spectrometry (FT-ICR-MS). Strong connection between $C_{20\text{-}33}H_hO_o$/$C_{18,30}H_hO_oN_n$ compounds in particles smaller than 0.10 μm and the VOCs emitted from local intertidal macroalgae suggests that the organic compounds (OC) in ultrafine particles are formed probably via the gas-phase oxidation of long-chain fatty aldehydes or acids, followed by particle-phase accretion reactions or imine formation during the coastal NPF events. In 0.18-0.56 μm particles, dominant $C_8$-$C_{20}$ CHO, CHON, CHOS and CHONS compounds (maximum: $C_{10}$ or $C_{15}$) are suggested most likely to be terpene oxidation products. Highly oxygenated compounds with $0.6 \leq H/C \leq 1.5$ and $0.67 \leq O/C \leq 1.2$ reside mostly in 0.18-0.56 μm particles, accounting for 5% of the OC formulas in this size range. Iodinated OC are subsequently formed via electrophilic substitution of non-iodinated OC by iodine cations in iodine-rich particles. CHN and Cl/Br-containing OC account altogether for only 1-4% of total OC intensity. As a result of the above compound distribution, the intensity weighted unsaturation degree and carbon oxidation state of OC increase with particle size. The distribution of aromatic compounds (i.e. Aromaticity Index > 0.5) is bimodal with peaks in 0.056-0.18 μm and 1.0-3.2 μm. In addition, our study observed higher unsaturation degree, carbon oxidation state and aromaticity of OC in coastal $PM_{2.5}$ than inland urban $PM_{2.5}$ in the same region.


## 1 Introduction

Organic aerosols (OA) contributes 20%-90% of submicron aerosol mass in the troposphere (Jimenez et al., 2009; Zhang et al., 2007). The OA in coastal atmosphere is expected to be more diverse than continental OA due to the contributions from both continental and marine sources. Unlike the deeper understanding of continental OA, the OA from marine sources is less investigated and thus poorly quantified in aerosol-cloud-climate models. The seawater contains a complex mixture of dissolved organic matter (DOM) including amino acids, proteins, fatty acids, carbohydrates and humic-type components etc. (Garrett, 1967; Hansell & Carlson, 2014; Liss & Duce, 1997). They are exported to marine aerosols primarily via the formation of sea spray aerosol (SSA) (Lapina et al., 2011; Prather et al., 2013). Direct marine volatile organic compound (VOC) emissions include biological vapor emissions from marine biota (Gašparović et al., 1998; Žutić et al., 1981) and abiotic production of functionalized VOCs from sea surface microlayer (Brüggemann et al., 2018; Carpenter & Nightingale, 2015; Chiu et al., 2016). Subsequent photochemistry of these VOCs may lead to marine and coastal secondary OA (SOA) formation.

Halogen (Cl, Br and I) is a group of non-negligible atmospheric constituents in both gas and aerosol phases. Their sources include sea salt aerosols (Finlayson-Pitts, 2003; Rossi, 2003), halogenated methane emission from the ocean (Gribble, 1992; Mosher et al., 1993), biomass burning (Rahn et al., 2006) and fossil fuel combustion (Maenhaut et al., 1993; Xu et al., 2005). There have been many studies of halogen

chemistry in the stratosphere and the troposphere, however, mainly focusing on their atmospheric sources, cycle mechanisms, the reactivity of halogen atoms towards VOC and ozone depletion mechanism (Farman et al., 1985; Peter, 1996; Riva et al., 2015; Tham et al., 2016; Thornton et al., 2010; Wang et al., 2017a; Wennberg et al., 1994). , So far, Cl/Br/I-containing organic compounds (OC) in aerosol particles are seldom reported (Wang & Ruiz, 2017; Wang et al., 2020), altought they may play an important role in regulating the recycling of active halogens from particles to gas phase.

Traditionally, Gas Chromatography or Liquid Chromatography-Mass Spectrometry (GC-MS or LC-MS) were widely used in the offline molecular characterization of OA. Electron ionization instruments like Aerosol Mass Spectrometry (SP-AMS) and Aerosol Chemical Speciation Monitor (ACSM) have also been widely used to provide fragment ion information of both inorganic and organic components in complex aerosol samples (Canagaratna et al., 2007; DeCarlo et al., 2006). Soft ionization techniques like Chemical Ionization (CI), Electrospray Ionization (ESI) and EESI (Extractive ESI) interfaced with High Resolution (HR)-MS such as Time-of-Flight (ToF)-MS, Orbitrap-MS, Fourier transform-ion cyclotron resonance MS (FT-ICR-MS) (Laskin et al., 2018) make it possible to examine molecular ions of OA, either online or offline, in laboratory experiments (Kundu et al., 2012; Putman et al., 2012), field campaigns (Lin et al., 2012; Mazzoleni et al., 2012; O'Brien et al., 2014; Wang et al., 2016; Willoughby et al., 2016) or specific emission sources (Cui et al., 2019; Fleming et al., 2017; Laskin et al., 2009). One of the recent hot topics arising from the application of online CI-APi-TOF is the investigation of highly oxygenated organic molecules (HOM), which are believed to play an important role in SOA formation and new particle formation (NPF) (Bianchi et al., 2019).

Herein, we reported size-resolved molecular characteristics of OA collected at a coastal NPF hotspot in east China coastline. We presented a comprehensive analysis of elemental composition, carbon number distribution, oxidation degree, unsaturation degree, aromaticity and the content of highly oxygenated compounds (HOC) of organic elemental groups with a high size resolution. VOC emission from local coastal macroalgae was measured with Solid Phase Micro-Extraction (SPME)-GC-MS technique to assist in interpreting the sources and formation mechanism of OA. Chemical composition of bulk aerosol particles was also compared between coastal and urban $PM_{2.5}$ in the region to obtain a better understanding of OA in the context of severe PM pollution in China.

## 2 Materials and Methods

### 2.1 Sample collection

Size-resolved coastal aerosol particles were collected at Xiangshan gulf (29°29′ N, 121°46′ E) of east China, a coastal NPF hotspot where iodine-induced NPF (I-NPF) occurred regularly from spring to summer (Yu et al., 2019). The sampling site is about 40 and 200 m away from at high tide and low tide, respectively. 13-stage nano Micro-Orifice Uniform Deposit Impactor (nano-MOUDI, MSP Corp, Shoreview, MN) was used with 50% aerodynamic cutoff sizes 18, 10, 5.6, 3.2, 1.8, 1.0, 0.56, 0.32, 0.18, 0.10,

0.056, 0.032, 0.018, and 0.010 μm. Pre-baked Aluminum foil filters were used as sampling substrate to reduce the adsorption of gaseous species. In order to reduce potential particle-bounce artifacts, two nano-MOUDI were placed side by side to collect 0.010-0.10 μm particles (on stages 10-13; other stages were silicon greased) and 0.10-18 μm particles (on stages 1-9) separately. The sampling lasted continuously for 72 hours from 9-11 May 2018 when NPF occurred daily, so that particle chemical composition of the NPF events can be obtained from offline analyses. Afterwards one set of field blank samples was collected alike, but with a high efficiency particulate air (HEPA) filter being placed at the gas inlet of nano-MOUDI. Particle number size distribution during the period is shown in Figure S1. Detailed information of PNSD measurement could be found in Yu et al. (2019).

A 23-hour $PM_{2.5}$ sample was collected onto 90 mm diameter pre-baked quartz fiber filter in another I-NPF day from 27-28 April 2018 at the same site. To make comparison, a 23-hour $PM_{2.5}$ sample was collected simultaneously at an inland urban site (32°20′ N, 118°71′ E) in Nanjing, a megacity in the same region (Yangtze River Delta region). The urban sampling site is located at the third floor (15m above the ground level) of an academic building on the Nanjing University of Information Science and Technology (NUIST) campus. $PM_{2.5}$ samples were collected using a median-volume aerosol sampler (TH-150C, Wuhan Tianhong Ltd., China) at a flow rate of 100 L $min^{-1}$. Field blank filters were collected at both sites. All samples were stored at −20 °C in a refrigerator until chemical analysis.

## 2.2 ESI-FT-ICR-MS

Half of a MOUDI filter or one quarter of a $PM_{2.5}$ filter was extracted by ultrasonication in an ice-water bath for 40 min with 10 mL mixed solvent (1:1 v/v water and methanol; LCMS grade) and was filtered through a 0.2 μm PTFE membrane syringe filter. The extract was dried using a rotary evaporator below 40 °C and redissolved in 0.5 mL water. Sample solution was directly infused into an ESI-FT-ICR-MS (SolariX XR 9.4T instrument, Bruker Daltonics, Coventry, UK) at a flow rate of 180 μL $h^{-1}$. ESI source conditions were as follows: nebulizer gas pressure 1 bar; dry gas pressure 4 bar and its temperature 200 °C; capillary voltage 4.5 kV. Ion accumulation time in argon-filled hexapole collision pool with 1.5 V of direct current voltage and 1400 Vp-p of radio frequency (RF) amplitude was 0.05 s, followed by transporting ions through a hexapole ion guide to the ICR cell for 0.7 ms. 4 M words of data were recorded over the mass range of 150-1000 for each run. A total of 128 scans were collected to enhance signal/noise (S/N) ratio and dynamic range. The OC analysis was conducted only for aerosol particles smaller than 3.2 μm. The extracts of 10-18 nm sample and 18-32 nm sample were combined to enhance the sensitivity of OC detection in small particle sizes. Field blank samples were treated following the same procedure.

A resolving power ($m/\Delta m_{50\%}$) 550,000 at m/z 300 of the FT-ICR-MS allows the determination of possible formulas for singly charged molecular ions. Only m/z values between 150-1000 Th that satisfies S/N > 10 were considered. Formula assignment fulfils the following criteria (Fuller et al., 2012; Mazzoleni et al., 2012): molecular

formulas are restricted to $C_{1\text{-}50}H_{1\text{-}100}X_{0\text{-}3}N_{0\text{-}5}O_{1\text{-}50}S_{0\text{-}2}$ in ESI- mode and $C_{1\text{-}50}H_{1\text{-}100}X_{0\text{-}3}N_{0\text{-}50}O_{0\text{-}50}$ in ESI+ mode (X= Cl/Br/I); mass tolerance is ±0.5 ppm. H/C, O/C, and N/C ratios are limited to 0.3-3, 0-3 and 0-1.3 in the ESI+ mode. H/C, O/C, N/C and S/C ratios are limited to 0.3-3, 0-3, 0-0.5 and 0-0.2 in the ESI- mode. Isotopologue-containing formulas are removed from the formula lists. A formula with m/z > 500 is not reported if it did not belong to any $CH_2$ homologous series. S, Cl and Br containing formulas are assigned only if their isotope patterns match with the theoretical ones. Formula calculation was done following the same procedure for the field blank samples. All formulas found in the field blank samples, regardless of peak intensity, were excluded from the formula lists of real samples.

To evaluate the degree of unsaturation and oxidation state of a molecular formula $C_cH_hX_xN_nO_oS_s$, double bond equivalent (DBE) and carbon oxidation state (OSC) are calculated as follows (Kroll et al., 2011; Mazzoleni et al., 2012; Minerath & Elrod, 2009)：

$$\mathrm{DBE} = 1 + 0.5 \times (2c - h + n - x) \quad (1)$$

$$OSC = 2 \times \frac{o}{c} - \frac{h}{c} \quad (2)$$

DBE was required to be non-negative. To evaluate the degree of unsaturation or oxidation state of a group of molecular formulas in a sample, relative intensity (RI) weighted $(\mathrm{DBE/C})_w$ and $\mathrm{OSC}_w$ are calculated as:

$$(\mathrm{DBE/C})_w = \sum \mathrm{RI}_i \times (\mathrm{DBE/C})_i \,/ \sum \mathrm{RI}_i \quad (3)$$

$$\mathrm{OSC}_w = \sum \mathrm{RI}_i \times \mathrm{OSC}_i \,/ \sum \mathrm{RI}_i \quad (4)$$

where $\mathrm{RI}_i$, $(\mathrm{DBE/C})_i$ and $\mathrm{OSC}_i$ are the RI, DBE/C and OSC of an individual molecular formula i in a sample.

Aromaticity index (AI) of a molecular formula is calculated as

$$\mathrm{AI} = \frac{\mathrm{DBE_{AI}}}{\mathrm{C_{AI}}} = \frac{1+c-o-s-0.5h}{c-o-s-n} \quad (5)$$

For the formulas detected in the ESI- mode, half of the oxygen (O) atoms are assumed to be associated with σ-bond. Equation (5) is then modified to $\mathrm{AI} = \frac{\mathrm{DBE_{AI}}}{\mathrm{C_{AI}}} = \frac{1+c-0.5o-s-0.5h}{c-0.5o-s-n}$. If $\mathrm{DBE_{AI}} \leq 0$ or $C_{AI} \leq 0$, then AI = 0. Threshold value of $\mathrm{AI} \geq 0.5$ provides unambiguous minimum criteria for the presence of aromatic structure in a molecule (Koch & Dittmar, 2006; Yassine et al., 2014).

We define highly oxygenated compound (HOC) as a compound with $0.6 < \mathrm{H/C} \leq 1.5$,$0.67 \leq \mathrm{O/C} \leq 1.2$ according to its position in a Van Krevelen diagram (Ning et al., 2019; Wozniak et al., 2008; Wu et al., 2019). Apparently, HOC is not equivalent to HOMs, which is defined by Bianchi et al. (2019) as high O/C molecules formed via gas phase autoxidation reaction. Nevertheless, HOC can be used as a proxy to show the intensity and size distribution of HOMs in aerosol particles.

## 2.3 SP-AMS

Half of each quartz fiber filter was extracted, dried and redissolved in 20 mL water, as above, for $PM_{2.5}$ bulk chemical composition analysis by using a Soot Particle-AMS (Aerodyne Research Inc., Massachusetts, USA). The aliquot of $PM_{2.5}$ sample solution was atomized by an aerosol atomizer (TSI Model 3076) and dehumidified to RH less than 10% through a diffusion dryer filled with silica-gel before entering the SP-AMS. The aerosols in the sample flow were thermally vaporized at 600 °C using a resistively heated tungsten vaporizer. The resulting vapor was ionized in an EI source (70ev). The SP-AMS was switched between a high sensitive V-mode and a high mass resolution W-mode. The m/z range was ∼1000 for V-mode and ∼450 for W-mode, respectively. In this study, we used only W-mode data for characterization of non-refractory components in the $PM_{2.5}$ samples. The relative ionization efficiencies (RIE) of sulfate, nitrate, organics, ammonium and chloride were 1.2, 1.1, 1.4, 3.8 and 1.0, respectively. Field blank samples were treated alike. Detailed procedures for offline analysis of PM chemical composition using SP-AMS can be found in Ge et al. (2017) and Sun et al. (2010).

## 2.4 SPME-GC-MS

Fresh macroalgae (*Undaria pinnatifida*) was collected from intertidal zone at Xiangshan gulf and stored at -20 ℃ until the SPME-GC-MS analysis of the VOCs emitted by the algae. About 0.5 g algae was capped in a 20 mL headspace vial, where the emitted VOCs were extracted onto 100 μm polydimethylsiloxane (PDMS) coated fiber (Supelco, Bellefonte, PA, USA) at 60 °C and an agitation speed of 500 rpm for 40 min equilibration time on an automatic injection platform (MPS, Gerstel, Germany). The fiber was then removed from the headspace vial and inserted into the injection port of a GC-MS apparatus (GCMS-QP2010 Plus, Shimadzu). The compounds on the fiber were desorbed for 2 min at 280 °C in the injection port operated in splitless mode. Carrier gas was He with a flow rate of 1.5 mL $min^{-1}$. The analytes were separated in a Rtx-5MS capillary column (30 m, 0.25 mm i.d. 0.25 μm film of 5% diphenyl-polysiloxane and 95% dimethyl-polysiloxane). Oven temperature program was held at 50 °C for 2 min, ramped to 230 °C at the rate of 20 °C $min^{-1}$, ramped to 280 °C at 2.5 °C $min^{-1}$ and held for 2 min. MS conditions were as follows: EI 70 eV, interface temperature 240 °C, ion source 220 °C, solvent delay time 1 min. MS detector was operated in full scan mode, by scanning a mass range of m/z 10-450. The most probable identities of the analytes were obtained based on the best matching score by comparing with the reference mass spectra in the NIST library.

## 3 Results and Discussion

### 3.1 $PM_{2.5}$ bulk chemical composition

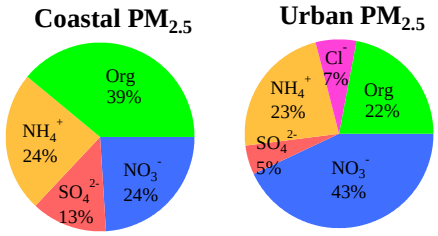


**Figure 1**. Mass contributions of organics (Org), sulfate ($SO_4^{2-}$), nitrate ($NO_3^-$), ammonium ($NH_4^+$) and chloride ($Cl^-$) in coastal $PM_{2.5}$ (left) and urban $PM_{2.5}$ (right).

Figure 1 shows a comparison of $PM_{2.5}$ bulk chemical composition between the coastal site and the urban site measured by offline SP-AMS. Coastal $PM_{2.5}$ contains a higher OA and $SO_4^{2-}$ mass fraction than urban $PM_{2.5}$, probably due to stronger primary emission or high conversion ratio of precursor vapors (like $SO_2$, dimethyl sulfide and other VOCs) at the coast site (Andreae, 1990; Kettle et al., 1999). On the contrary, urban $PM_{2.5}$ contains more $NO_3^-$ (43% vs. 24%) and $Cl^-$ (7% vs. 0%) than coastal $PM_{2.5}$. Nitrate is the end product of $NO_x$ photochemistry that is expected to be more active in urban atmosphere (Liao et al., 2004). The higher mass fraction of $Cl^-$ in urban $PM_{2.5}$ is probably a result of primary $Cl^-$ emission from fossil fuel combustion. The absence of $Cl^-$ in coastal $PM_{2.5}$ indicates that $Cl^-$ is probably abundant in coarse-mode sea salt aerosols (SSA), but not in fine particles.

### 3.2 Molecular formula assignments

The formulas detected as deprotonated species in the ESI- mode are grouped into 7 subgroups based on their elemental composition: $CHO^-$, $CHON^-$, $CHOS^-$, $CHONS^-$, iodine containing OC ($I\text{-}OC^-$), chloride containing OC ($Cl\text{-}OC^-$) and bromine containing OC ($Br\text{-}OC^-$). The subgroups in the ESI+ mode include 6 subgroups ($CHO^+$, $CHON^+$, $CHN^+$, $I\text{-}OC^+$, $Cl\text{-}OC^+$ and $Br\text{-}OC^+$) detected as protonated species and 2 subgroups (CHO+Na and CHON+Na) detected as sodium adducts. We show the formula numbers of each OC subgroup in Table 1, as well as their relative contributions to total OC intensity in the $PM_{2.5}$ samples and size-resolved coastal samples in Figure 2b and 2c.

Size-dependent OC formula number and total intensity show a bimodal distribution in coastal aerosols (Figure 2a). Surprisingly high formula number and total intensity in < 56 nm particles are obviously attributed to intense NPF events during the sampling period. Another peak of OC number and total intensity is in 0.32-0.56 μm particles, after which OC decreases rapidly with particle size. Organic composition of coastal aerosols is highly size-dependent and high similarities are only seen in neighboring size bins (e.g., 0.18-0.32 μm and 0.32-0.56 μm, < 32 nm and 32-56 nm). This can be seen in Table S1 showing the repeatability of molecular formulas in any two of nine size bins. One exception is the OC in 0.56-1.0 μm particles.

261 **Table 1.** *Formula numbers of subgroups for size-resolved coastal aerosols, coastal $PM_{2.5}$ and urban $PM_{2.5}$ in both ESI+ and ESI- modes.*

| | < 0.032 μm | 0.032-0.056 μm | 0.056-0.10 μm | 0.10-0.18 μm | 0.18-0.32 μm | 0.32-0.56 μm | 0.56-1.0 μm | 1.0-1.8 μm | 1.8-3.2 μm | Coastal $PM_{2.5}$ | Urban $PM_{2.5}$ |
|---|---|---|---|---|---|---|---|---|---|---|---|
| | | | | | ESI- mode | | | | | | |
| $CHO^-$ | 518 | 561 | 146 | 370 | 505 | 473 | 241 | 37 | 18 | 937 | 1023 |
| $CHON^-$ | 929 | 620 | 216 | 271 | 329 | 344 | 106 | 23 | 25 | 754 | 2176 |
| $CHOS^-$ | 162 | 208 | 59 | 211 | 230 | 369 | 110 | 38 | 22 | 657 | 628 |
| $CHONS^-$ | 126 | 107 | 34 | 93 | 79 | 118 | 21 | 11 | 10 | 217 | 555 |
| $I\text{-}OC^-$ | 89 | 93 | 22 | 56 | 17 | 15 | 12 | 8 | 17 | 625 | 36 |
| $Cl\text{-}OC^-$ | 24 | 5 | 7 | 7 | 0 | 0 | 0 | 1 | 0 | 2 | 35 |
| $Br\text{-}OC^-$ | 0 | 0 | 0 | 0 | 0 | 1 | 0 | 0 | 0 | 3 | 0 |
| Total | 1850 | 1594 | 484 | 1008 | 1160 | 1320 | 490 | 118 | 92 | 3195 | 4453 |
| | | | | | ESI+ mode | | | | | | |
| $CHO^+$ | 43 | 101 | 20 | 109 | 239 | 338 | 92 | 3 | 10 | 611 | 316 |
| CHO+Na | 165 | 284 | 310 | 181 | 118 | 21 | 67 | 103 | 96 | 523 | 1116 |
| $CHON^+$ | 437 | 467 | 225 | 372 | 717 | 713 | 178 | 36 | 27 | 2162 | 1544 |
| CHON+Na | 782 | 681 | 635 | 210 | 118 | 25 | 48 | 58 | 36 | 445 | 1315 |
| $CHN^+$ | 15 | 14 | 17 | 18 | 3 | 2 | 3 | 2 | 5 | 17 | 24 |
| $I\text{-}OC^+$ | 48 | 127 | 47 | 77 | 27 | 15 | 26 | 48 | 58 | 682 | 21 |
| $Cl\text{-}OC^+$ | 1 | 3 | 2 | 2 | 2 | 0 | 0 | 1 | 1 | 8 | 11 |
| $Br\text{-}OC^+$ | 1 | 0 | 0 | 0 | 0 | 0 | 0 | 0 | 1 | 0 | 4 |
| Total | 1335 | 1542 | 1196 | 920 | 1150 | 1104 | 402 | 247 | 229 | 4055 | 3828 |
| | | | | | Summary | | | | | | |
| Non-halogen OC | 2629 | 2549 | 1535 | 1640 | 2003 | 2163 | 804 | 307 | 248 | 5052 | 6847 |
| I-OC | 124 | 200 | 68 | 123 | 39 | 28 | 34 | 53 | 68 | 1203 | 56 |
| Cl-OC | 25 | 8 | 9 | 9 | 2 | 0 | 0 | 2 | 1 | 10 | 46 |
| Br-OC | 1 | 0 | 0 | 0 | 0 | 1 | 0 | 0 | 1 | 3 | 4 |

262

36-87% of the formulas in 0.56-1.0 μm particles are also present in < 0.56 μm particles. The results imply that the OC in 0.56-1.0 μm particles, to some extent, originated from smaller particles.

Among 6953 formulas in coastal $PM_{2.5}$ and 6271 formulas in urban $PM_{2.5}$, nearly half of them (3526) were commonly found in both samples. Coastal $PM_{2.5}$ sample and size-resolved MOUDI samples were both collected during I-NPF days at the same site and are thus expected to have similar composition. However, only 3009 formulas are commonly present in $PM_{2.5}$ (6953 formulas in total) and size-resolved samples (6013 formulas in total). More specifically, 83-89% of OC formulas in 0.18-1.0 μm particles are also present in coastal $PM_{2.5}$, but only 43-57 % of OC formulas in < 0.1 μm particles and 35-38% in > 1.0 μm particles are present in coastal $PM_{2.5}$ (Table S1). This suggests that the $PM_{2.5}$ sampling offers an approach to assess the chemical composition of only submicron particles (0.18-1.0 μm), not ultrafine (< 0.1 μm) or supermicron (> 1.0 μm) particles.

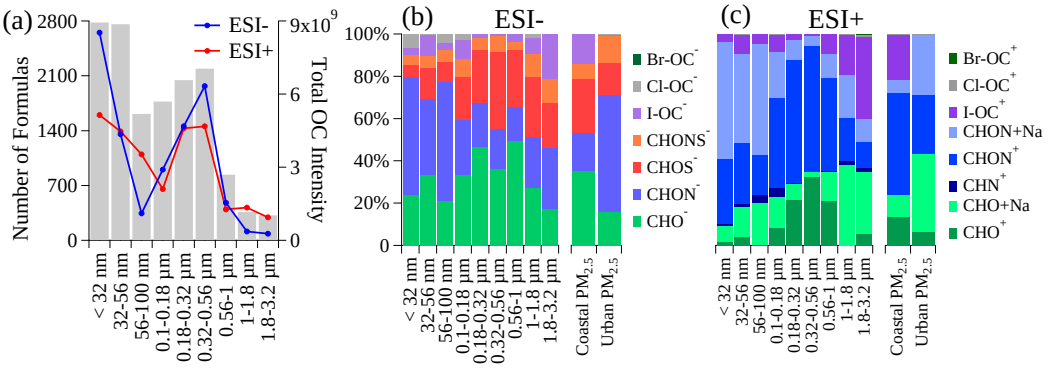


**Figure 2**. (a) The number (grey bars) and total intensity (blue and red lines for ESI- and ESI+ modes, respectively) of OC in size-resolved coastal aerosols. (b) Intensity fraction of 7 subgroups in ESI- mode. (c) Intensity fraction of 8 subgroups in ESI+ mode.

### 3.3 Size-dependent molecular characteristics and sources of OC subgroups

Size-dependent carbon number distribution, $OSC_w$, $(DBE/C)_w$ and aromaticity are shown in Figure 3 for all OC subgroups in size-resolved coastal aerosols. The comparison of these parameters between coastal $PM_{2.5}$ and urban $PM_{2.5}$ is shown in Figure 4.

#### 3.3.1 CHO compounds

CHO subgroup is the second largest contributor of OC in coastal ultrafine particles. In general, the fraction of CHO in total OC intensity increases with particle size (Figure 2). The intensity distribution of $CHO^-$ compounds is bimodal in terms of particle size (Figure 3a), being dominated by $C_{20,24,28,32}$ and $C_{21,25,29,33}$ in < 56 nm particles and $C_{10\text{-}20}$ in 0.18-0.56 μm particles. The intensity distribution of $CHO^+$ compounds is unimodal dominated by $C_{12\text{-}18}$ species in 0.18-0.56 μm particles (Figure 3a). The $(DBE/C)_w$ and $OSC_w$ values of CHO compounds are higher in submicron particles than those in ultrafine particles (Figure 3b). The percentage of aromatic compounds (i.e. AI > 0.5) in CHO subgroup is below 10% and increases with particle size.

The intensity fraction of CHO compounds in urban $PM_{2.5}$ (16%) is lower than that in coastal $PM_{2.5}$ (35%) in the ESI- mode, but the opposite is observed in the ESI+ mode (urban vs. coastal: 43% vs. 25%). The carbon numbers of CHO compounds in urban $PM_{2.5}$ are higher than (or close to) those of coastal $PM_{2.5}$ (Figure 4a): $C_{15\text{-}22}$ (maximum: $C_{20}$) and $C_{20\text{-}33}$ (maximum: $C_{26}$) subclasses are prominent in $CHO^-$ and CHO+Na compounds of urban $PM_{2.5}$, while $C_{9\text{-}20}$ (maximum: $C_{10}$) and $C_{13\text{-}16}$ (maximum: $C_{15}$) subclasses are prominent in $CHO^-$ and $CHO^+$ compounds of coastal $PM_{2.5}$. Unsaturation degree, carbon oxidation state and the percentage of aromatic compounds are lower in urban $PM_{2.5}$ than in coastal $PM_{2.5}$ (Figure 4b).

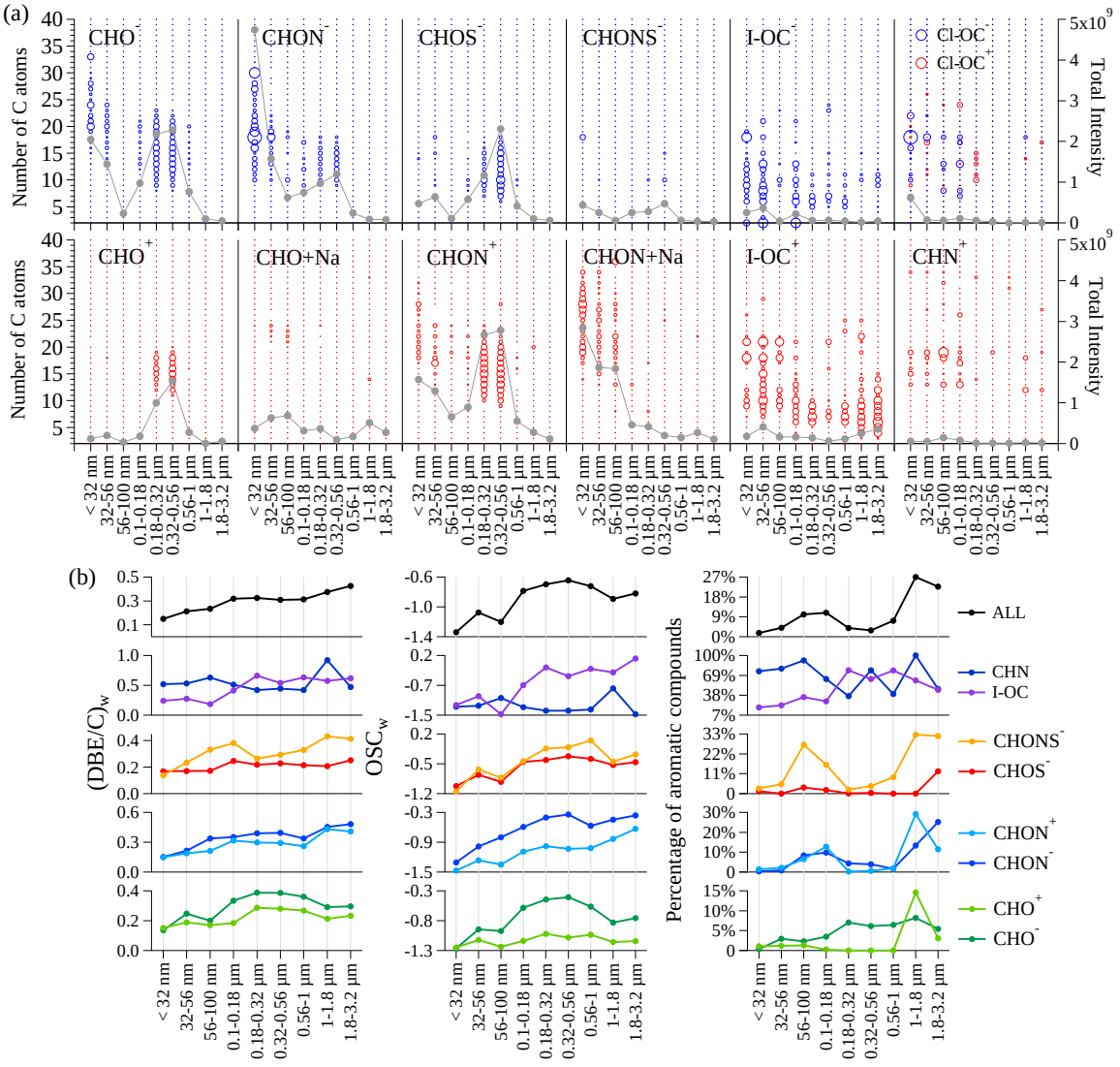


**Figure 3**. (a) Carbon number distributions (circles) and total intensity (gray lines) for each OC subgroup in size-resolved coastal aerosols. Circle size is proportional to the relative intensities of molecular formulas on a logarithmic scale. Note that the circle sizes of $CHN^+$, $I\text{-}OC^-$, $I\text{-}OC^+$, $Cl\text{-}OC^+$ and $Cl\text{-}OC^-$ subgroups are not scaled proportionally with other subgroups, due to their

relatively small intensities. (b) Intensity weighted OSC, DBE/C and the percentage of aromatic compounds with AI > 0.5 for subgroups and all OC formulas.

To assess the sources of CHO compounds at the coastal NPF hotspot, we compare the OC formulas in ultrafine, submicron and supermicron size ranges with those in ozonolysis products of biogenic terpenes (terpene SOA), cooking OA (COA) and biomass burning OA (BBOA) reported in the literature (Table 2). It shows that 15%-27%, 48-62% and 7-16% of total CHO intensity in ultrafine, submicron and supermicron particles can be attributed to identical molecular formulas detected in ozonolysis products of isoprene (Nguyen et al., 2010), α-pinene (Putman et al., 2012), d-limonene (Kundu et al., 2012) and β-caryophyllene (Kundu et al., 2017). Out of 69 CHO formulas detected in food cooking emission by Reyes-Villegas et al. (2018), 9, 33 and 5 formulas are observed in the ultrafine, submicron and supermicron particles collected at the coastal site, respectively. Among them are typical COA tracer linoleic acid ($C_{18}H_{32}O_2$), vernolic acid ($C_{18}H_{32}O_3$) and arachidonic acid ($C_{20}H_{32}O_2$) (He et al., 2010). Fleming et al. (2017) reported 28 CHO formulas in aerosol particles collected from brushwood burning smoke. Among them, 5, 12 and 3 formulas are observed in the ultrafine, submicron and supermicron particles at the coastal site, respectively, including typical biomass burning phenolic tracers such as $C_{14}H_{16}O_4$ and $C_{14}H_{16}O_3$. In summary, terpene SOA is the major contributor to the CHO compounds in submicron particles, and its contribution is less important in ultrafine and supermicron particles.

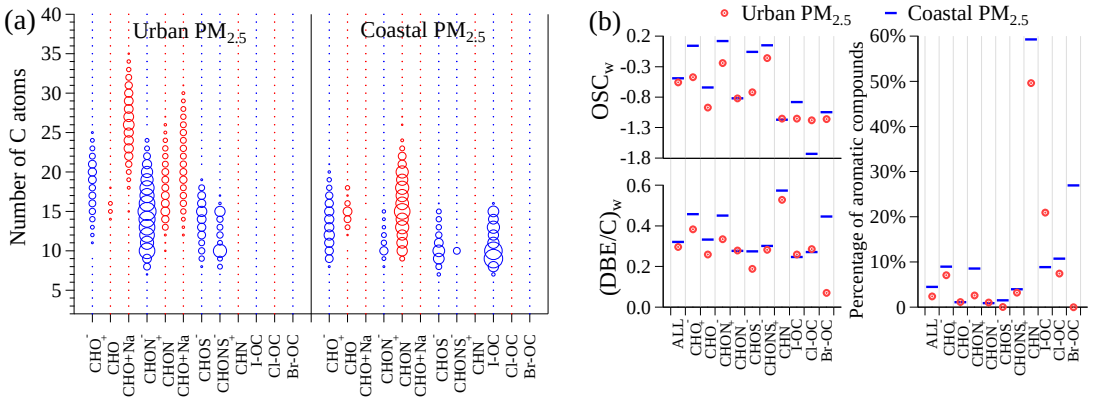


**Figure 4**. (a) Carbon number distribution for OC subgroups in urban $PM_{2.5}$ and coastal $PM_{2.5}$. (b) Comparison of $(DBE/C)_w$, $OSC_w$ and the percentage of aromatic compounds between urban $PM_{2.5}$ and coastal $PM_{2.5}$.

Interestingly, a total of 26 $C_{20,24,28,32}H_hO_{3\text{-}8}$ and $C_{21,25,29,33}H_hO_{4\text{-}8}$ formulas with DBE =1, which are not found in the terpene SOA, COA or BBOA above, make up approximately 32% of the total intensity of $CHO^-$ formulas in ultrafine particles. The most prominent formulas among them are of 4 or 6 O atoms. The interval of 4 carbon number of these formulas suggests they may be organic accretion reaction products of $C_{20}$ and $C_4$ precursors in particle phase. The VOC emission measurement from local macroalgae supports this hypothesis. Total ion chromatogram produced by SPME-GC-MS analysis is shown in Figure 5. The 15 most notable peaks are $C_4$ butyraldehyde and butane-2,3-diol, $C_{8,9}$ fatty alcohols, $C_{9,11,12,20,21}$ fatty aldehydes and $C_{14,18,20,22}$ fatty acids. The formation of the most abundant CHO compounds $C_{20,24,28,32}H_hO_{4,6}$ in the ultrafine particles is thus proposed from the reaction of the most abundant $C_{20}$ icosanal and $C_4$ precursors (butyraldehyde and butane-2,3-diol). A three-step Scheme I is shown in Figure 6: first, the

autoxidation of icosanal and subsequent reaction with $RO_2$ produce $C_{20}$ hydroxyaldehydes. Second, low-volatility $C_{20}$ hydroxyaldehydes condense onto nano-particles to form particle-phase $C_{20}$ hydroxyaldehydes, their hydrolysis products, as well as $C_{24}$ α,β-unsaturated aldehydes via the aldol condensation with butyraldehyde. Third, $C_{28,32}$ acetal or hemiacetal formation between all above aldehyde products and butane-2,3-diol .

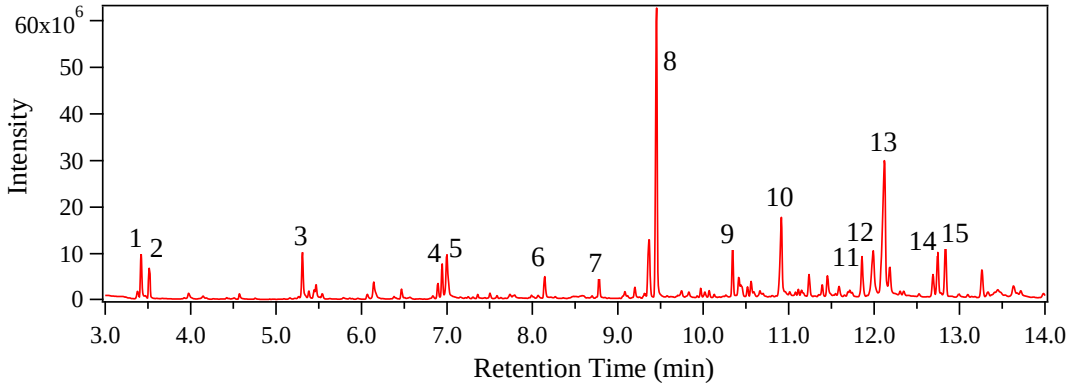


**Figure 5**. Total ion chromatogram of macroalgae (*Undaria pinnatifida*) emission: 1. Butyraldehyde, 2. Butane-2,3-diol, 3. Amyl vinyl carbinol, 4. 2-Nonenal, 5. 2-Nonen-1-ol, 6. Undecanal, 7. Dodecanal, 8. Icosanal, 9. Henicosanal, 10. Tetradecanoic acid, 11. Petroselinic acid, 12. Stearic acid, 13. Linolenic acid, 14. Eicosapentaenoic acid, 15. Docosahexaenoic acid.

The end products of Scheme I are the eight most abundant $C_{20,24,28,32}$ polyhydroxy alcohols with one C=C or C=O bond and 4 or 6 O atoms. The formation of other similar products with 3, 5, 7 and 8 O atoms are also possible if the number of added O atoms is varying in the gas phase oxidation intermediates. $C_{21,25,29,33}$ $H_hO_{4\text{-}8}$ can be formed similarly from their precursor $C_{21}$ henicosanal. In our previous study, we have confirmed that the NPF events at this coastal NPF hotspot were induced by iodine species (Yu et al., 2019). In this work, we further establish the relationship between the OC in ultrafine particles and the VOCs emitted from local intertidal macroalgae. These VOCs are thus most likely emitted mutually with iodine or iodomethanes from the macroalgae, although iodine or iodomethanes were not observed by the SPME-GC-MS technique.

### 3.3.2 CHON compounds

CHON is the most abundant subgroup in ultrafine particles, accounting for 53 % and 80% of total OC intensity in the ESI- and ESI+ modes respectively (Figure 2). The fraction of CHON in total OC intensity decreases with particle size. $CHON^-$ and CHON+Na are characterized by significant peaks around $C_{18,30}$, and $C_{20,28}$ in < 32 nm particles, respectively. $CHON^+$ is dominated by $C_{10\text{-}20}$ peaks (maximum: $C_{15}$) in 0.18-0.56 μm particles (Figure 3a). The $(DBE/C)_w$ and $OSC_w$ of CHON compounds increase generally with particle size. The percentage of aromatic compounds exhibits a bimodal size distribution with peaks in 0.056-0.18 μm (~10%) and 1.0-3.2 μm (~30%) (Figure 3b).

**Table 2.** *Number (n) and carbon number distribution of identical OC formulas detected both in size-resolved coastal aerosols and potential sources. Also shown is the percentage of total OC intensity that can be attributed to those identical molecular formulas. The last column shows the MS techniques used to detect the OC formulas from potential sources.*

| Potential source | Ultrafine | submicron | Supermicron | MS technique |
|---|---|---|---|---|
| | | CHO | | |
| Isoprene ozonolysis[a] | n=139 (15%), $C_{8,15,20}$ | n=408 (48%), $C_{9,15,20}$ | n=31 (12%), $C_{11,16,21}$ | LTQ-Orbitrap MS |
| α-pinene ozonolysis[b] | n=136 (15%), $C_{9,15,20,23}$ | n=354 (44%), $C_{9,15,20,24}$ | n=21 (7%), $C_{8,15,19}$ | |
| Limonene ozonolysis[c] | n=145 (16%), $C_{9,15,20}$ | n=361 (45%), $C_{9,15,19}$ | n=20 (7%), $C_{8,15,19}$ | FT-ICRMS |
| β-carypohyllene ozonolysis[d] | n=235 (27%), $C_{9,14,19,24}$ | n=497 (62%), $C_{9,15,19,24}$ | n=43 (16%), $C_{11,16}$ | |
| Food cooking emission[e] | n=9, $C_{8,9,12,16-18,20,21}$ | n=33, $C_{6,8-14,16-18,21}$ | n=5, $C_{9,11,12,17,21}$ | FIGAERO−ToF-CIMS |
| Brushwood burning emission[f] | n=5, $C_{12,13,18}$ | n=12, $C_{10-14,18}$ | n=3, $C_{10-13}$ | LTQ-Orbitrap MS |
| | | CHON | | |
| α-pinene ozonolysis ($NO_x$)[g] | n=8, $C_{10}$ | n=28, $C_{7-10}$ | n=3, $C_{10}$ | FIGAERO ToF-CIMS |
| Brushwood burning emission[f] | n=10, $C_{10-14}$ | n=21, $C_{7,10-15}$ | n=1, $C_{13}$ | LTQ-Orbitrap MS |
| | | S-containing formulas | | |
| Nine monoterpenes SOA[h] | n=6, $C_{9-10}$ | n=19, $C_{7-10}$ | n=9, $C_{7-10}$ | UPLC/ESI-TOF MS |
| β-caryophyllene SOA[i] | n=9, $C_{9,14-16}$ | n=14, $C_{9,14-16}$ | n=1, $C_9$ | |
| | | CHN | | |
| Brushwood burning emission[f] | n=3, $C_{13-14}$ | n=3, $C_{13}$ | ND | LTQ-Orbitrap MS |
| Crop biomass burning emission[j] | n=2, $C_{13}$ | n=3, $C_{13}$ | ND | |
| | Formulas tentatively attributed to algae emission | | | |
| The reaction of $C_{18}$ fatty acid and $C_{20,21}$ fatty aldehydes in macroalgae emission | $C_{20,24,28,32}H_hO_o$, $C_{21,25,29,33}H_hO_o$, DBE=1: n=26 (32%) | $C_{20,24,28,32}H_hO_o$, $C_{21,25,29,33}H_hO_o$, DBE=1: n=7 (0.4%) | $C_{20,24,28,32}H_hO_o$, DBE=1: n=2 (7%) | SPME-GC-MS |
| | $C_{18,30}H_hO_oN_n$, DBE=1-4: n=78 (36%) | $C_{18,30}H_hO_oN_n$, DBE=1-4: n=22 (6%) | $C_{18,30}H_hO_oN_n$, DBE=1-4: n=3 (8%) | |

*Note*. a. Nguyen et al. (2010), b.Putman et al. (2012), c. Kundu et al. (2012), d. Kundu et al. (2017) e. Reyes-Villegas et al. (2018), f. Fleming et al. (2017), g. Lee et al. (2016), h.Surratt et al. (2008), i. Chan et al. (2010), j. Wang et al. (2017b).

CHON compounds in urban $PM_{2.5}$ contain more carbon atoms than those in coastal $PM_{2.5}$ (Figure 4a). The most abundant C number subclasses of $CHON^-$, $CHON^+$ and CHON+Na formulas are $C_{15}\backslash C_{15}\backslash C_{19}$ and $C_{10}\backslash C_{15}\backslash C_{15}$ in urban and coastal $PM_{2.5}$, respectively. The $(DBE/C)_w$, $OSC_w$ and the percentage of aromatic compounds in urban $PM_{2.5}$ are lower than those in coastal $PM_{2.5}$, which are consistent with CHO compounds (Figure 4b).

Nitrogen atoms in CHON compounds could exist as either oxidized form ($-NO_2$ or $-ONO_2$) or reduced form (e.g. amine and imine). The average O/N ratios of CHON formulas in size-resolved aerosols are shown in Figure S2. No matter in ESI+ or ESI- mode, CHON formulas in the submicron particles have higher average O/N ratios (2.3-5.7) than ultrafine particles (3.2-6.8)

and supermicron particles (2.4-5.3). This implies there are more amine or imine-containing CHON compounds in the ultrafine and supermicron particles than in the submicron particles. 78 $C_{18,30}H_hO_oN_n$ formulas with DBE=1-4 contribute 36% of the total intensity of $CHON^-$ formulas in ultrafine particles. $C_{18,30}H_hO_oN_n$ are also the most abundant formulas among all OC formulas detected in the coastal aerosols (Figure 3a). Among them, at least 47 formulas should contain at least one amine or imine group, because their O atom numbers or DBE values are not large enough to allow the assignment of $–NO_2$ for all N atoms. On the other hand, we note that there is no N-containing compound in the VOCs emitted from the macroalgae sample (Figure 5). This leads to the conclusion that the reduced-N atoms in $C_{18,30}H_hO_oN_n$ compounds must be from atmospheric reactions.

The most plausible formation mechanism of $C_{18,30}H_hO_oN_n$ with DBE=1-4 is proposed to stem from linolenic acid (the highest abundant organic acid in the algae emission), ammonia and $C_{12}$ fatty aldehyde in a 3-step Scheme II (Figure 6): first, OH and $O_2$ addition to C=C double bonds of linolenic acid and subsequent reaction with $RO_2$ form oxygenated $C_{18}$ fatty acids containing hydroxyl or carbonyl group. Second, those low-volatility $C_{18}$ products then condense onto aerosol particles and $C_{18}H_hO_oN_n$ compounds are formed via imine formation reactions with $NH_3$ or ammonolysis. Third, $C_{18}$ imine products react with another carbonyl-containing $C_{12}$ fatty aldehyde to form $C_{30}H_hO_oN_n$. It should be noted that the products in Scheme II include merely some of the most abundant formulas detected in the ultrafine particles. Other $C_{18}$ and $C_{30}$ products with 3-8 O atoms are possible, given the unsaturation degree of $C_{18}$ fatty acid precursors and the extent of oxygen addition in the gas phase are varying. In addition, $C_{20,28}H_hO_oN_n$ compounds detected in the ESI+ mode might be formed similarly via imine formation reactions between $NH_3$ and the carbonyl-containing $C_{20,28}H_hO_o$ products formed in Scheme I.

As shown in Table 2, 33 CHON formulas are commonly found in field and α-pinene chamber experiments by Lee et al. (2016). They are supposed to be organic nitrate products initiated by nitrate radical ($NO_3$) or by $O_3$ or OH in the presence of $NO_x$. Among them, we find 28 $C_{7\text{-}10}$ compounds in submicron particles, but only 8 and 3 $C_{10}$ compounds in ultrafine and supermicron particles, respectively. Fleming et al. (2017) reported 150 CHON formulas in aerosol particles collected from brushwood burning smokes. Among them, 10, 21 and 1 formulas are observed in the ultrafine, submicron and supermicron particles at our coastal site, respectively. These results indicate that being compared to ultrafine aerosol particles, the CHON compounds in submicron particles are largely attributed to terpene SOA products in the high NOx condition or biomass burning smokes.

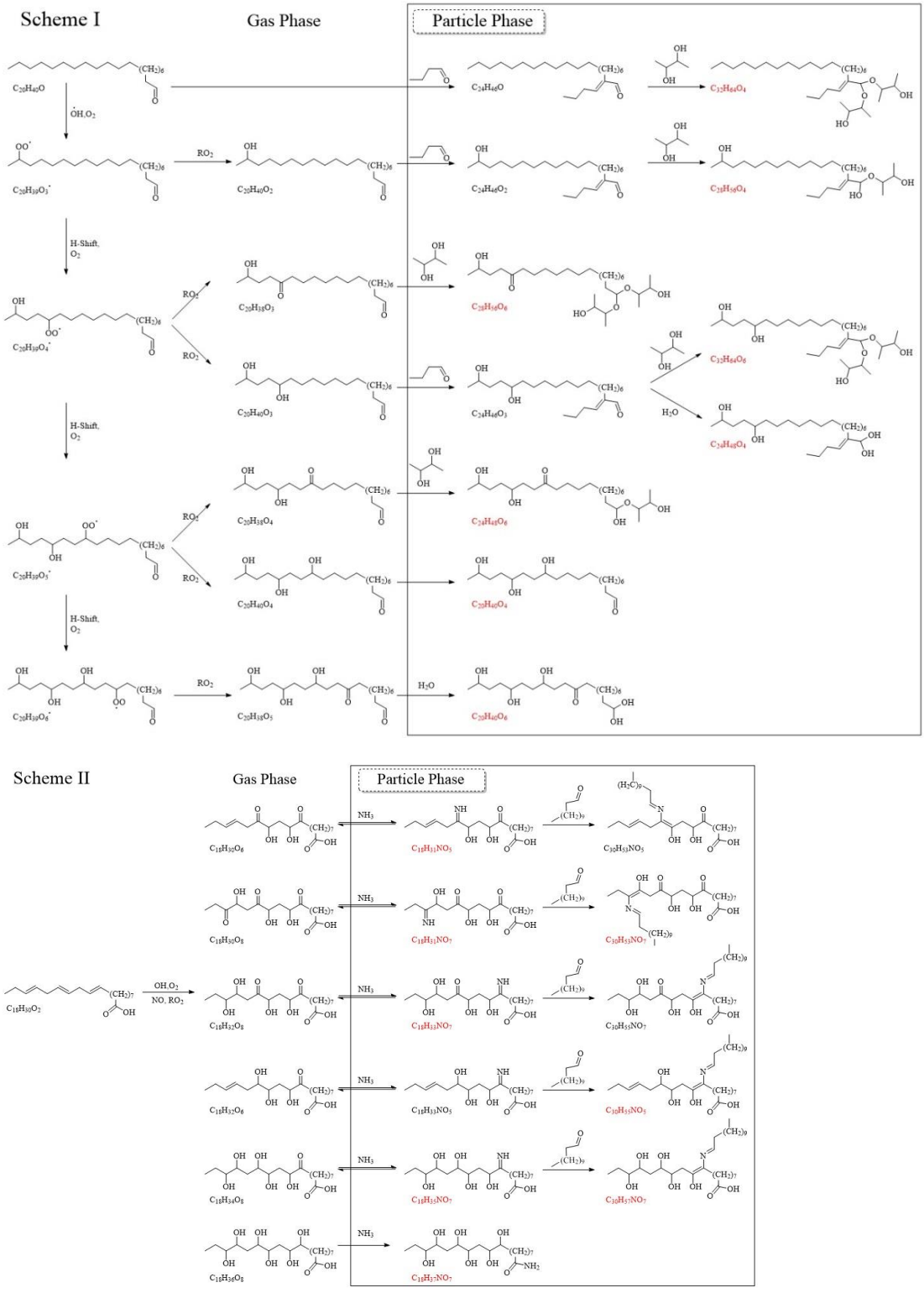


**Figure 6**. Scheme I: formation mechanism of $C_{20,24,28,32}H_hO_o$ (DBE=1) species from icosanal emission; Scheme II: formation mechanism of $C_{18,30}H_hO_oN_n$ (DBE=1-4) species from linolenic acid emission. Formulas in red were detected by FT-ICR-MS.

### 3.3.3 S-containing compounds (CHOS and CHONS)

The total intensity of CHOS formulas is 2.6 times on average that of CHONS formulas in size-resolved coastal aerosols. The size distribution of S-containing compounds is unimodal dominated by $C_{8\text{-}18}$ species (maximum: $C_{10}$) in 0.18-0.56 μm particles (Figure 3a). More than 90% of CHOS or CHONS formulas in size-resolved aerosol particles have O/S ratios greater than 4. 50%, 83% and 57% of CHONS compounds have O/S ratios greater than 7 in ultrafine, submicron and supermicron particles, respectively, implying the existence of nitrooxy-organosulfates. In general, the $(DBE/C)_w$ and $OSC_w$ of S-containing compounds increase with particle size. Similar to CHON, the percentage of aromatic compounds in CHOS and CHONS subgroups exhibits a bimodal size distribution with peaks in 0.056-0.10 μm and 1.0-3.2 μm (Figure 3b).

S-containing compounds accounted for 33% and 28% of total OC intensity (ESI- mode, Figure 2b) in coastal and urban $PM_{2.5}$, respectively. The most abundant C number subclass of S-containing compounds are $C_{10}$ in coastal $PM_{2.5}$, while carbon number shift more to $C_{15}$ in urban $PM_{2.5}$ (Figure 4a). $(DBE/C)_w$, $OSC_w$ and the percentage of aromatic compounds in S-containing compounds in urban $PM_{2.5}$ are again lower than those in coastal $PM_{2.5}$ (Figure 4b).

Surratt et al. (2008) and Chan et al. (2010) conducted a series of photooxidation experiments on 9 monoterpenes and β–caryophyllene in the presence of acidified sulfate seed aerosols, respectively (Table 2). They identified 36 CHOS and 16 CHONS formulas in the products (Chan et al., 2010; Surratt et al., 2008). Among them, 14, 32 and 9 formulas are observed in our coastal ultrafine, submicron and supermicron particles, respectively. 35 and 34 of them are observed in coastal $PM_{2.5}$ and urban $PM_{2.5}$, respectively, including two most abundant compounds $C_{10}H_{17}NO_{10}S$ and $C_{10}H_{17}NO_9S$. This suggests that S-containing compounds in our sites were probably formed via the reactions of CHO and CHON compounds with sulfate in the aerosol particles.

### 3.3.4 CHN compounds

A total of 42 CHN formulas are observed in size-resolved coastal aerosols, accounted for less than 4% of the total OC intensity in each size bin. CHN formulas are dominated by $C_{13\text{-}20}$ species in ultrafine particles (Figure 3a), among which $C_{19}H_{23}N_3$, $C_{15}H_{13}N_3$ and $C_{18}H_{20}N_6$ are the most abundant formulas. 17 and 24 CHN formulas accounted for less than 0.5% of the total OC intensity in coastal $PM_{2.5}$ and urban $PM_{2.5}$, respectively. The most abundant formulas in coastal $PM_{2.5}$ are $C_{20}H_{11,13}N_7$ and $C_{29}H_{29}N_3$, while the most abundant one in urban $PM_{2.5}$ is $C_{27}H_{25,27,29}N_3$. All these high-intensity formulas had AI values > 0.5, indicating the possible presence of benzene rings or heterocyclic amines in their molecular structures (Song et al., 2018; Sun et al., 2010).

$(DBE/C)_w$ and $OSC_w$ of CHN formulas show relatively small variation with particle size (Figure 3b), except for 1.0-1.8 μm particles. On the other hand, a strong variation with particle size is seen for the percentage of aromatic compounds. Among all the subgroups in the coastal aerosols, CHN formulas possess relatively high $(DBE/C)_w$, low $OSC_w$ and high percentage of aromatic compounds. These three parameters in urban $PM_{2.5}$ are again lower than those in coastal $PM_{2.5}$ (Figure 4b).

CHN compounds, also known as alkaloids, have been proved as the main composition of BBOA by the previous studies (Laskin et al., 2009; Lin et al., 2012; Magda et al., 2012; Samy et al., 2013). Fleming et al. (2017) and Wang et al. (2017b) identified 101 and 74 CHN formulas, respectively, in the burning emissions of brushwood, straw, corn and wheat. However, only 5 of

them ($C_{13}H_{10,24}N_2$, $C_{14}H_{18}N$ and $C_{13}H_{11,19}N_3$) are found in ultrafine and submicron particles at the coastal site. Another five formulas $C_{10}H_{14}N_2$, $C_{11,15}H_{20}N_2$, $C_{14}H_{18,20}N_2$ and $C_{10}H_{14}N_2$ are found in the $PM_{2.5}$ samples. This indicates that the burning emissions of these biomass materials play a minor role in the formation of OC in coastal and urban aerosol particles.

3.3.5 Halogen-containing organic compounds

There are 1216 and 106 halogen-containing formulas in coastal $PM_{2.5}$ and urban $PM_{2.5}$, respectively. The vast difference of halogen-containing formula numbers between coastal $PM_{2.5}$ and urban $PM_{2.5}$ is due to the different numbers of I-OC formulas.

**I-OC** There are 450 I-OC formulas in total detected in size-resolved coastal aerosols, less than 1203 I-OC formulas in coastal $PM_{2.5}$, indicating positive artifacts are formed via chemical reactions between iodine and OC in coastal $PM_{2.5}$. The size distribution of I-OC is bimodal (Figure 3a). Those in ultrafine particles include (1) nine $C_{18}H_hO_oN_nI$ formulas with DBE = 1-4, (2) $C_9H_{16}NO_3I$ and its $C_{10}$-$C_{13}$ homologues, (2) diiodo acetic acid $C_2H_2O_2I_2$, diiodomethane $CH_2I_2$, (3) iodinated $C_{21}$ carbonyls $C_{21}H_{39}OI$ and $C_{21}H_{41}OI$, (4) iodinated $C_{21,25,27,29}$ alcohols or ethers with DBE = 0, (5) iodinated $C_{10}$ and $C_{15}$ terpene and sesquiterpene oxidation products and (6) iodinated organic sulfate $C_8H_{17}N_2SO_8I$ and $C_{21}H_{43}SO_4I$. The I-OC in supermicron particles are dominated by $C_{4\text{-}10}$ species, the most abundant of which are iodinated $C_4$-$C_6$ CHO and CHON compounds with DBE = 3-6. Therefore, I-OC is most likely formed in iodine-rich particles via electrophilic substitution of aromatic hydrogen or α-H of carbonyl and carboxyl groups in non-iodine compounds by iodine cations (probably from HOI or $I_2$).

The 1203 I-OC formulas in coastal $PM_{2.5}$ accounted for 14% and 21% of total OC intensity in the ESI- and ESI+ modes, respectively. On the contrary, 56 I-OC formulas in urban $PM_{2.5}$ accounted for only 0.2% and 0.1% of total OC intensity in the two ESI modes. These results indicate that the coastal site is an emission hotspot of aerosol particles rich in organic iodine compounds.

**Cl/Br-OC** 10 and 46 Cl-OC formulas are detected in coastal $PM_{2.5}$ and urban $PM_{2.5}$, respectively, account for less than 0.5% of the total OC intensity in both samples. More Cl-OC formulas in urban is consistent with the higher $Cl^-$ content observed by using SP-AMS. These Cl species arose probably from the combustion of fossil fuels or biomass in the urban areas. A total of 50 Cl-OC formulas (S/N: 10.7-1164) is observed in the size-resolved coastal samples. 25 Cl-OC formulas are detected in < 0.032 μm particles, among which $C_{18}H_{36}ClNO_2$ is the most abundant one. The number of Cl-OC formulas decreases with increasing particle size. Wang et al. (2020) studied chlorine-initiated oxidation of alpha-pinene in the presence of NOx in chamber experiments. $C_{10}H_{15}ClO_{5\text{-}6}$ detected in urban $PM_{2.5}$ fits well to the reaction mechanism proposed by Wang et al. (2020).

Virtually no prior studies have reported Br-OC in aerosol particles. Only 3, 3 and 4 Br-OC formulas are found in the MOUDI samples, coastal $PM_{2.5}$ and urban $PM_{2.5}$, respectively. The total intensity of Br-OC is one order of magnitude lower than that of Cl-OC. The 10 Br-OC formulas (S/N: 10.7-27.4), as well as the Cl-OC with S/N over 100, are listed in Table S2. Br-OC can be either from primary emission in aerosol particles or the reaction of reactive bromine species towards organic compounds in the atmosphere. It thus seems that both pathways are not effective for the formation of Br-OC.

## 3.4 Highly Oxygenated Compounds (HOC)

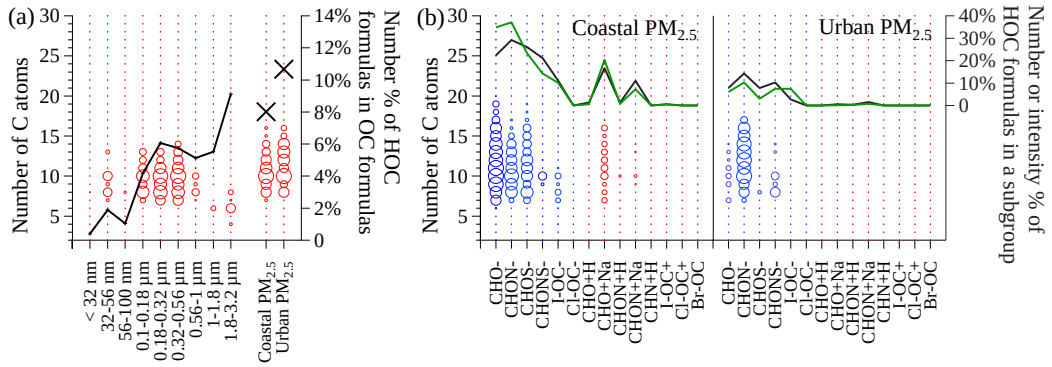


**Figure 7**. (a) Carbon number distribution of HOC formulas (circles) and the number percentage of HOC formulas in OC formulas of a sample. (b) The number percentage (green lines), intensity percentage (black lines) and carbon number distributions (red and blue circles) of HOC formulas in a subgroup of coastal $PM_{2.5}$ and urban $PM_{2.5}$ sample.

HOC are dominated by $C_{7\text{-}13}$ species (maximum: $C_{10}$) in submicron particles from 0.1 µm to 0.56 µm (Figure 7a). 69, 170 and 34 formulas are assigned to HOC in ultrafine, submicron and supermicron particles, respectively, contributing < 2%, 5% and 5-8% of the formulas in the three size ranges. Our data lead to the conclusion that organic compounds in aged submicron particles are more oxygenated than those in fresh ultrafine particles.

742 and 502 HOC formulas are observed in coastal $PM_{2.5}$ and urban $PM_{2.5}$, contributing 8% and 11% of total formulas in the two samples, respectively (Figure 7a). The total intensity of HOC in coastal $PM_{2.5}$ is higher than urban $PM_{2.5}$ (Figure 7b). This indicates a higher oxidation degree of OC in coastal $PM_{2.5}$ than urban $PM_{2.5}$. In terms of elemental subgroup, 20% to 37% of $CHO^-$, $CHON^-$, $CHOS^-$ and CHO+Na formulas are HOC in coastal $PM_{2.5}$, while only 10% of $CHON^-$ formulas are HOC in urban $PM_{2.5}$. HOC in coastal $PM_{2.5}$ and urban $PM_{2.5}$ have similar carbon number distribution that is dominated by $C_{8\text{-}15}$ species (maximum: $C_{10}$).

## 4 Conclusions

We conducted a comprehensive analysis of elemental composition, unsaturation degree, carbon oxidation state and aromaticity of coastal OA with a high size resolution. A systematical comparison of bulk $PM_{2.5}$ chemical composition between a coastal NPF hotspot and a typical inland urban site was shown in the context of severe PM pollution in the Yangtze River Delta region of China. Our analysis shows that the molecular composition of organic aerosols is highly size-dependent at the coastal NPF hotspot, including the OC in ultrafine particles generated in NPF events, secondary products of terpene oxidation in aged submicron particles and the OC in sea salt particles. The analysis based on size-resolving sampling technique and ultrahigh resolution MS helps to understand the molecular characteristics and sources of organic aerosols. On the contrary, $PM_{2.5}$ sampling is subject to both the loss of ultrafine particle components due to lower collection efficiency and positive artifacts formed via post-sampling reactions among aerosol components (e.g. I-OC).

Based on the measurement of VOC emission from local intertidal macroalgae, dominant $C_{20\text{-}33}H_hO_o$ and $C_{18,30}H_hO_oN_n$ compounds in particles < 0.10 µm are proposed to form via gas-

phase oxidation of $C_{20,21}$ fatty aldehydes and $C_{18}$ fatty acids, followed by organic accretion reaction with small aldehyde/alcohol in aerosol particles. The presence of abundant reduced-N atoms in the OC of this size range suggests the involvement of ammonia via imine formation reaction. On the other hand, CHO, CHON, CHOS and CHONS compounds in 0.18-0.56 μm submicron particles are dominated by $C_8$-$C_{20}$ peaks (maximum: $C_{10}$ or $C_{15}$). They can be most likely attributed to terpene SOA products by comparing with previous chamber experiment studies. Submicron particles also accommodate most of highly oxygenated compounds. Organic iodine compounds are suggested to form via electrophilic substitution of all above compounds by iodine cations in iodine-rich particles. In total, CHN and Cl/Br-containing OC only accounted for 1-4% of total OC intensity of organic aerosols at this coastal NPF hotspot site.

## Acknowledgments and Data

The work was supported by the National Science Foundation of China (grant numbers 41975831 and 41675124), the National Key Research and Development Program of China (grant number 2016YFC0203100) and Survey of China Project (grant numbers 1212011120281 and 1212011120274)

Data availability: datasets for this research are available in the in-text data citation reference Yu et al. (2020)

## References

Andreae, M. O. (1990). Ocean-atmosphere interactions in the global biogeochemical sulfur cycle. *Marine Chemistry, 30*, 1-29. doi:10.1016/0304-4203(90)90059-L

Bianchi, F., Kurtén, T., Riva, M., Mohr, C., Rissanen, M. P., Roldin, P., et al. (2019). Highly Oxygenated Organic Molecules (HOM) from Gas-Phase Autoxidation Involving Peroxy Radicals: A Key Contributor to Atmospheric Aerosol. *Chemical Reviews*, *119*(6), 3472-3509. doi:10.1021/acs.chemrev.8b00395

Brüggemann, M., Hayeck, N. & George, C. (2018). Interfacial photochemistry at the ocean surface is a global source of organic vapors and aerosols. *Nature Communications, 9*. doi:10.1038/s41467-018-04528-7

Canagaratna, M. R., Jayne, J. T., Jimenez, J. L., Allan, J. D., Alfarra, M. R., Zhang, Q., et al. (2007). Chemical and microphysical characterization of ambient aerosols with the aerodyne aerosol mass spectrometer. *Mass spectrometry reviews*, *26*(2), 185-222. doi:10.1002/mas.20115

Carpenter, L. & Nightingale, P. (2015). Chemistry and Release of Gases from the Surface Ocean. *Chemical reviews*, *115*. doi:10.1021/cr5007123

Chan, M. N., Surratt, J., Chan, A., Schilling, K., Offenberg, J., Lewandowski, M., et al. (2010). Influence of aerosol acidity on the chemical composition of Secondary Organic Aerosol from β-caryophyllene. *Atmospheric Chemistry and Physics Discussions, 10*. doi:10.5194/acpd-10-29249-2010

590 Chiu, R., Tinel, L., Gonzalez, L., Ciuraru, R., Bernard, F., George, C. & Volkamer, R. (2016). UV
591 Photochemistry of Carboxylic Acids at the Air ‐ Sea Boundary: A Relevant Source of Glyoxal
592 and other OVOC in the Marine Atmosphere. *Geophysical Research Letters*, *44*.
593 doi:10.1002/2016GL071240

594 Cui, M., Li, C., Chen, Y., Zhang, F., Li, J., Jiang, B., et al. (2019). Molecular characterization of
595 polar organic aerosol constituents in off-road engine emissions using Fourier transform ion
596 cyclotron resonance mass spectrometry (FT-ICR MS): implications for source apportionment.
597 *Atmospheric Chemistry and Physics*, *19*(22), 13945-13956. doi:10.5194/acp-19-13945-2019

598 DeCarlo, P. F., Kimmel, J. R., Trimborn, A., Northway, M. J., Jayne, J. T., Aiken, A. C., et al.
599 (2006). Field-deployable, high-resolution, time-of-flight aerosol mass spectrometer. *Anal Chem*,
600 *78*(24), 8281-8289. doi:10.1021/ac061249n

601 Farman, J. C., Gardiner, B. G. & Shanklin, J. D. (1985). Large Losses of Total Ozone in Antarctica
602 Reveal Seasonal ClOx/NOx Interaction. *Nature*, *315*, 207-210. doi:10.1038/315207a0

603 Finlayson-Pitts, B. J. (2003). The Tropospheric Chemistry of Sea Salt: A Molecular-Level View
604 of the Chemistry of NaCl and NaBr. *Chemical Reviews*, *103*(12), 4801-4822.
605 doi:10.1021/cr020653t

606 Fleming, L., Lin, P., Laskin, A., Laskin, J., Weltman, R., Edwards, R., et al. (2017). Molecular
607 Composition of Particulate Matter Emissions from Dung and Brushwood Burning Household
608 Cookstoves in Haryana, India. *Atmospheric Chemistry and Physics Discussions*, 1-35.
609 doi:10.5194/acp-2017-784

610 Fuller, S. J., Zhao, Y., Cliff, S. S., Wexler, A. S. & Kalberer, M. (2012). Direct Surface Analysis
611 of Time-Resolved Aerosol Impactor Samples with Ultrahigh-Resolution Mass Spectrometry.
612 *Analytical Chemistry*, *84*(22), 9858-9864. doi:10.1021/ac3020615

613 Garrett, W. D. (1967). The organic chemical composition of the ocean surface. *Deep Sea Research*
614 *and Oceanographic Abstracts*, *14*(2), 221-227. doi:10.1016/0011-7471(67)90007-1

615 Gašparović, B., Kozarac, Z., Saliot, A., Ćosović, B. & Möbius, D. (1998). Physicochemical
616 Characterization of Natural andex-SituReconstructed Sea-Surface Microlayers. *Journal of Colloid*
617 *and Interface Science*, *208*(1), 191-202. doi:10.1006/jcis.1998.5792

618 Ge, X., Li, L., Chen, Y., Chen, H., Wu, D., Wang, J., et al. (2017). Aerosol characteristics and
619 sources in Yangzhou, China resolved by offline aerosol mass spectrometry and other techniques.
620 *Environmental Pollution*, *225*, 74-85. doi:10.1016/j.envpol.2017.03.044

621 Gribble, G. W. (1992). Naturally Occurring Organohalogen Compounds--A Survey. *Journal of*
622 *Natural Products*, *55*(10), 1353-1395. doi:10.1021/np50088a001

623 Hansell, D. A. & Carlson, C. A. (2014), *Biogeochemistry of Marine Dissolved Organic Matter*,
624 Elsevier Science.

625 He, L. Y., Lin, Y., Huang, X., Guo, S., L, X., Su, Q., et al. (2010). Characterization of high-
626 resolution aerosol mass spectra of primary organic aerosol emissions from Chinese cooking and
627 biomass burning. *Atmospheric Chemistry and Physics*, *10*. doi:10.5194/acp-10-11535-2010

628 Jimenez, J. L., Canagaratna, M. R., Donahue, N. M., Prevot, A. S. H., Zhang, Q., Kroll, J. H., et
629 al. (2009). Evolution of Organic Aerosols in the Atmosphere. *Science*, *326*(5959), 1525-1529.
630 doi:10.1126/science.1180353

Kettle, A. J., Andreae, M. O., Amouroux, D., Andreae, T. W., Bates, T. S., Berresheim, H., et al. (1999). A global database of sea surface dimethylsulfide (DMS) measurements and a procedure to predict sea surface DMS as a function of latitude, longitude, and month. *Global Biogeochemical Cycles*, *13*(2), 399-444. doi:10.1029/1999gb900004

Koch, B. P. & Dittmar, T. (2006). From mass to structure: an aromaticity index for high-resolution mass data of natural organic matter. *Rapid Communications in Mass Spectrometry*, *20*(5), 926-932. doi:10.1002/rcm.2386

Kroll, J. H., Donahue, N. M., Jimenez, J. L., Kessler, S. H., Canagaratna, M. R., Wilson, K. R., et al. (2011). Carbon oxidation state as a metric for describing the chemistry of atmospheric organic aerosol. *Nature Chemistry*, *3*(2), 133-139. doi:10.1038/nchem.948

Kundu, S., fisseha, Putman, A., Rahn, T. & Mazzoleni, L. (2012). High molecular weight SOA formation during limonene ozonolysis: Insights from ultrahigh-resolution FT-ICR mass spectrometry characterization. *ATMOSPHERIC CHEMISTRY AND PHYSICS*, *12*. doi:10.5194/acp-12-5523-2012

Kundu, S., Fisseha, R., Putman, A. L., Rahn, T. A. & Mazzoleni, L. R. (2017). Molecular formula composition of β-caryophyllene ozonolysis SOA formed in humid and dry conditions. *Atmospheric Environment*, *154*, 70-81. doi:10.1016/j.atmosenv.2016.12.031

Lapina, K., Heald, C. L., Spracklen, D. V., Arnold, S. R., Allan, J. D., Coe, H., et al. (2011). Investigating organic aerosol loading in the remote marine environment. *Atmos. Chem. Phys.*, *11*(17), 8847-8860. doi:10.5194/acp-11-8847-2011

Laskin, A., Smith, J. S. & Laskin, J. (2009). Molecular Characterization of Nitrogen-Containing Organic Compounds in Biomass Burning Aerosols Using High-Resolution Mass Spectrometry. *Environmental science & technology*, *43*(10), 3764-3771. doi:10.1021/es803456n

Laskin, J., Laskin, A. & Nizkorodov, S. A. (2018). Mass Spectrometry Analysis in Atmospheric Chemistry. *Analytical Chemistry*, *90*(1), 166-189. doi:10.1021/acs.analchem.7b04249

Lee, B. H., Mohr, C., Lopez-Hilfiker, F. D., Lutz, A., Hallquist, M., Lee, L., et al. (2016). Highly functionalized organic nitrates in the southeast United States: Contribution to secondary organic aerosol and reactive nitrogen budgets. *Proceedings of the National Academy of Sciences*, *113*(6), 1516. doi:10.1073/pnas.1508108113

Liao, H., Seinfeld, J. H., Adams, P. J. & Mickley, L. J. (2004). Global radiative forcing of coupled tropospheric ozone and aerosols in a unified general circulation model. *Journal of Geophysical Research: Atmospheres*, *109*(D16). doi:10.1029/2003jd004456

Lin, P., Rincon, A., Kalberer, M. & Yu, J. (2012). Elemental Composition of HULIS in the Pearl River Delta Region, China: Results Inferred from Positive and Negative Electrospray High Resolution Mass Spectrometric Data. *Environmental science & technology*, *46*, 7454-7462. doi:10.1021/es300285d

Liss, P. S. & Duce, R. A. (1997), *The Sea Surface and Global Change*, Cambridge University Press, Cambridge, doi:10.1017/CBO9780511525025.

Maenhaut, W., Kauppinen, E. I. & Lind, T. M. (1993). Study of size-fractionated coal-combustion aerosols using instrumental neutron activation analysis. *Journal of Radioanalytical and Nuclear Chemistry*, *167*(2), 259-269. doi:10.1007/BF02037185

672 Magda, C., Reinhilde, V., Farhat, Y., Yadian, G.-G., Xuguang, C., Willy, M., et al. (2012).
673 Chemical characterisation of humic-like substances from urban, rural and tropical biomass burning
674 environments using liquid chromatography with UV/vis photodiode array detection and
675 electrospray ionisation mass spectrometry. *Environmental Chemistry* (3), 273-284.
676 doi:10.1071/EN11163

677 Mazzoleni, L. R., Saranjampour, P., Dalbec, M. M., Samburova, V., Hallar, A. G., Zielinska, B.,
678 et al. (2012). Identification of water-soluble organic carbon in non-urban aerosols using ultrahigh-
679 resolution FT-ICR mass spectrometry: organic anions. *Environmental Chemistry*, *9*(3), 285-297.
680 doi:10.1071/EN11167

681 Minerath, E. & Elrod, M. (2009). Assessing the Potential for Diol and Hydroxy Sulfate Ester
682 Formation from the Reaction of Epoxides in Tropospheric Aerosols. *Environmental science &*
683 *technology*, *43*, 1386-1392. doi:10.1021/es8029076

684 Mosher, B., Winkler, P. & Jaffrezo, J.-L. (1993). Seasonal aerosol chemistry at Dye 3, Greenland.
685 *Atmospheric Environment. Part A. General Topics*, *27*, 2761-2772. doi:10.1016/0960-
686 1686(93)90308-L

687 Nguyen, T. B., Bateman, A. P., Bones, D. L., Nizkorodov, S. A., Laskin, J. & Laskin, A. (2010).
688 High-resolution mass spectrometry analysis of secondary organic aerosol generated by ozonolysis
689 of isoprene. *Atmospheric Environment*, *44*(8), 1032-1042. doi:10.1016/j.atmosenv.2009.12.019

690 Ning, C. P., Gao, Y., Zhang, H. J., Yu, H. R., Wang, L., Geng, N. B., et al. (2019). Molecular
691 characterization of dissolved organic matters in winter atmospheric fine particulate matters
692 (PM2.5) from a coastal city of northeast China. *Sci. Total. Environ.*, *689*(1), 312-321.
693 doi:10.1016/j.scitotenv.2019.06.418

694 O'Brien, R. E., Laskin, A., Laskin, J., Rubitschun, C. L., Surratt, J. D. & Goldstein, A. H. (2014).
695 Molecular characterization of S- and N-containing organic constituents in ambient aerosols by
696 negative ion mode high-resolution Nanospray Desorption Electrospray Ionization Mass
697 Spectrometry: CalNex 2010 field study. *Journal of Geophysical Research: Atmospheres*, *119*(22),
698 12,706-712,720. doi:10.1002/2014jd021955

699 Peter, T. (1996), Formation mechanisms of polar stratospheric clouds, in *Nucleation and*
700 *Atmospheric Aerosols 1996*, edited by M. Kulmala and P. E. Wagner, pp. 280-291, Pergamon,
701 Amsterdam, doi:10.1016/B978-008042030-1/50067-6.

702 Prather, K. A., Bertram, T. H., Grassian, V. H., Deane, G. B., Stokes, M. D., DeMott, P. J., et al.
703 (2013). Bringing the ocean into the laboratory to probe the chemical complexity of sea spray
704 aerosol. *Proceedings of the National Academy of Sciences*, *110*(19), 7550-7555.
705 doi:10.1073/pnas.1300262110

706 Putman, A. L., Offenberg, J. H., Fisseha, R., Kundu, S., Rahn, T. A. & Mazzoleni, L. R. (2012).
707 Ultrahigh-resolution FT-ICR mass spectrometry characterization of α-pinene ozonolysis SOA.
708 *Atmospheric Environment*, *46*, 164-172. doi:10.1016/j.atmosenv.2011.10.003

709 Rahn, K., Borys, R., Butler, E. & Duce, R. (2006). Gaseous and particulate halogens in the New
710 York City atmosphere*. *Annals of the New York Academy of Sciences*, *322*, 143-151.
711 doi:10.1111/j.1749-6632.1979.tb14123.x

712 Reyes-Villegas, E., Bannan, T., Le Breton, M., Mehra, A., Priestley, M., Percival, C., et al. (2018).
713 Online Chemical Characterization of Food-Cooking Organic Aerosols: Implications for Source

Apportionment. *Environmental science & technology*, *52*(9), 5308-5318. doi:10.1021/acs.est.7b06278

Riva, M., Healy, R. M., Flaud, P.-M., Perraudin, E., Wenger, J. C. & Villenave, E. (2015). Gas- and Particle-Phase Products from the Chlorine-Initiated Oxidation of Polycyclic Aromatic Hydrocarbons. *The Journal of Physical Chemistry A*, *119*(45), 11170-11181. doi:10.1021/acs.jpca.5b04610

Rossi, M. J. (2003). Heterogeneous Reactions on Salts. *Chemical Reviews*, *103*(12), 4823-4882. doi:10.1021/cr020507n

Samy, S., Robinson, J., Rumsey, I. C., Walker, J. T. & Hays, M. D. (2013). Speciation and trends of organic nitrogen in southeastern U.S. fine particulate matter (PM2.5). *Journal of Geophysical Research: Atmospheres*, *118*(4), 1996-2006. doi:10.1029/2012jd017868

Song, J., Li, M., Jiang, B., Wei, S., Fan, X. & Peng, P. a. (2018). Molecular Characterization of Water-Soluble Humic like Substances in Smoke Particles Emitted from Combustion of Biomass Materials and Coal Using Ultrahigh-Resolution Electrospray Ionization Fourier Transform Ion Cyclotron Resonance Mass Spectrometry. *Environmental science & technology*, *52*(5), 2575-2585. doi:10.1021/acs.est.7b06126

Sun, Y., Zhang, Q., C, A. & J, S. (2010). Insights into secondary organic aerosol formed via aqueous-phase reactions of phenolic compounds based on high resolution mass spectrometry. *Atmospheric Chemistry and Physics Discussions*, *10*. doi:10.5194/acpd-10-2915-2010

Surratt, J. D., Gómez-González, Y., Chan, A. W., Vermeylen, R., Shahgholi, M., Kleindienst, T. E., et al. (2008). Organosulfate formation in biogenic secondary organic aerosol. *J Phys Chem A*, *112*(36), 8345-8378. doi:10.1021/jp802310p

Tham, Y. J., Wang, Z., Li, Q., Yun, H., Wang, W., Wang, X., et al. (2016). Significant concentrations of nitryl chloride sustained in the morning: investigations of the causes and impacts on ozone production in a polluted region of northern China. *Atmos. Chem. Phys.*, *16*(23), 14959-14977. doi:10.5194/acp-16-14959-2016

Thornton, J. A., Kercher, J. P., Riedel, T. P., Wagner, N. L., Cozic, J., Holloway, J. S., et al. (2010). A large atomic chlorine source inferred from mid-continental reactive nitrogen chemistry. *Nature*, *464*(7286), 271-274. doi:10.1038/nature08905

Wang, D. S. & Ruiz, L. H. (2017). Secondary organic aerosol from chlorine-initiated oxidation of isoprene. *Atmos. Chem. Phys.*, *17*(22), 13491-13508. doi:10.5194/acp-17-13491-2017

Wang, H., Wang, X., Yang, X., Li, W., Xue, L., Tao, W., et al. (2017a). Mixed Chloride Aerosols and their Atmospheric Implications: A Review. *Aerosol and Air Quality Research*, *17*, 878–887. doi:10.4209/aaqr.2016.09.0383

Wang, X. K., Rossignol, S., Ma, Y., Yao, L., Wang, M. Y., Chen, J. M., et al. (2016). Molecular characterization of atmospheric particulate organosulfates in three megacities at the middle and lower reaches of the Yangtze River. *Atmospheric Chemistry and Physics*, *16*(4), 2285-2298. doi:10.5194/acp-16-2285-2016

Wang, Y., Riva, M., Xie, H., Heikkinen, L., Schallhart, S., Zha, Q., et al. (2020). Formation of highly oxygenated organic molecules from chlorine-atom-initiated oxidation of alpha-pinene. *Atmos. Chem. Phys.*, *20*(8), 5145-5155. doi:10.5194/acp-20-5145-2020

Wang, Y., Hu, M., Lin, P., Guo, Q., Wu, Z., Li, M., et al. (2017b). Molecular Characterization of Nitrogen-Containing Organic Compounds in Humic-like Substances Emitted from Straw Residue Burning. *Environmental science & technology*, *51*(11), 5951-5961. doi:10.1021/acs.est.7b00248

Wennberg, P. O., Cohen, R. C., Stimpfle, R. M., Koplow, J. P., Anderson, J. G., Salawitch, R. J., et al. (1994). Removal of Stratospheric O3 by Radicals: In Situ Measurements of OH, HO2, NO, NO2, ClO, and BrO. *Science*, *266*(5184), 398-404. doi:10.1126/science.266.5184.398

Willoughby, A. S., Wozniak, A. S. & Hatcher, P. G. (2016). Detailed Source-Specific Molecular Composition of Ambient Aerosol Organic Matter Using Ultrahigh Resolution Mass Spectrometry and 1H NMR. *Atmosphere.*, *7*(6), 79. doi:10.3390/atmos7060079

Wozniak, A. S., Bauer, J. E., Sleighter, R. L., Dickhut, R. M. & Hatcher, P. G. (2008). Technical Note: Molecular characterization of aerosol-derived water soluble organic carbon using ultrahigh resolution electrospray ionization Fourier transform ion cyclotron resonance mass spectrometry. *Atmos. Chem. Phys.*, *8*(17), 5099-5111. doi:10.5194/acp-8-5099-2008

Wu, C., Yang, J., Fu, Q., Zhu, B., Ruan, T. & Jiang, G. (2019). Molecular characterization of water-soluble organic compounds in PM2.5 using ultrahigh resolution mass spectrometry. *The Science of the total environment*, *668*, 917-924. doi:10.1016/j.scitotenv.2019.03.031

Xu, D., Dan, M., Song, Y., Chai, Z. & Zhuang, G. (2005). Concentration characteristics of extractable organohalogens in PM2.5 and PM10 in Beijing, China. *Atmospheric Environment*, *39*, 4119-4128. doi:10.1016/j.atmosenv.2005.03.030

Yassine, M. M., Harir, M., Dabek, E. & Schmitt-Kopplin, P. (2014). Structural characterization of organic aerosol using Fourier transform ion cyclotron resonance mass spectrometry: Aromaticity equivalent approach. *Rapid. Commun. Mass. Sp.*, *28*(22), 2445-2454. doi:10.1002/rcm.7038

Yu, Huan. (2020). Molecular Formulas of Organic Aerosols at Two Sites of East China [Data set]. Zenodo. http://doi.org/10.5281/zenodo.4016023

Yu, H., Ren, L. L., Huang, X. P., Xie, M. J., He, J. & Xiao, H. (2019). Iodine speciation and size distribution in ambient aerosols at a coastal new particle formation hotspot in China. *Atmos. Chem. Phys.*, *19*, 4025-4039. doi:10.5194/acp-19-4025-2019

Zhang, Q., Jimenez, J. L., Canagaratna, M. R., Allan, J. D., Coe, H., Ulbrich, I., et al. (2007). Ubiquity and dominance of oxygenated species in organic aerosols in anthropogenically-influenced Northern Hemisphere midlatitudes. *Geophysical Research Letters*, *34*(13). doi:10.1029/2007gl029979

Žutić, V., Ćosović, B., Marčenko, E., Bihari, N. & Kršinić, F. (1981). Surfactant production by marine phytoplankton. *Marine Chemistry*, *10*(6), 505-520. doi:10.1016/0304-4203(81)90004-9